Journal of Molecular Graphics and Modelling 50 (2014) 142–151

Contents lists available at ScienceDirect

Journal of Molecular Graphics and Modelling

journal homepage: www.elsevier.com/locate/JMGM

Molecular dynamics analysis of the interaction between the human BCL6 BTB domain and its SMRT, NcoR and BCOR corepressors: The quest for a consensus dynamic pharmacophore

J.M. Granadino-Roldán[a,*], C. Obiol-Pardo[b,c], M. Pinto[b,c], A. Garzón[d], J. Rubio-Martínez[b,c]

[a] Departamento de Química Física y Analítica, Universidad de Jaén, Campus "Las Lagunillas" s/n, 23071 Jaén, Spain
[b] Departament de Química Física, Universitat de Barcelona (UB), Martí iFranqués 1, 08028 Barcelona, Spain
[c] The Institut de Química Teòrica i Computacional (IQTCUB), Spain
[d] Facultad de Farmacia, Universidad de Castilla La Mancha, Paseo de los estudiantes, s/n, 02071 Albacete, Spain

ARTICLE INFO

Article history:
Accepted 4 April 2014
Available online 15 April 2014

Keywords:
BCL6
Molecular dynamics
Pharmacophore
Drug design
DLBCL

ABSTRACT

Targeting the BCL6 protein is a promising therapeutic strategy for the treatment of B cell lymphomas. One approach to treat these diseases consists of finding drug candidates able to disrupt the interactions established between BCL6 and its corepressors. Thus, this work presents a thorough comparative analysis of the interactions between the BCL6 BTB (bric-a-brac tramtrack broad complex) protein domain and its SMRT, NcoR and BCOR corepressor BBDs (BCL6 binding domain) through molecular dynamics. Moreover, a theoretical structure is presented and checked for the $BCL6^{BTB}$–$NcoR^{BBD}$ complex. Considering the BBDs to be composed of 17 amino acids, our analyses show the region involving residues 4–15 of these 17 to play a main role in the protein–corepressor interactions. Particularly SER^{11} seems to have a high relevance as it establishes specific bonds with $BCL6^{BTB}$ and is one of the only two residues sequence equivalent for the three studied corepressors. From this study, 14 pharmacophoric points have been proposed divided in two groups which coincide with residues 4–11 and 11–15, being SER^{11} a hinge point. This finding suggests the possibility of searching for 2 small molecule inhibitors, mimicking 8 and 7 pharmacophoric points, respectively, which could incorporate a hydrogen donor pharmacophoric point mimicking SER^{11} in any or both molecules. In short, the present work aims to contribute further knowledge in the modeling of drugs mimicking $BCL6^{BTB}$–corepressor complexes.

© 2014 Elsevier Inc. All rights reserved.

1. Introduction

The B-cell lymphoma 6 (BCL6) zinc-finger protein is a transcriptional repressor that regulates B-cell development [1], being required for mature B cells to form germinal centers (GCs) and undergo immunoglobulin affinity maturation [2,3]. BCL6 represses the transcription of genes involved in DNA damage responses, thereby enabling proliferation of GC B cells that are undergoing DNA deletions and mutations [4–7]. Its expression is downregulated at the end of the GC reaction [8]. BCL6 overexpression blocks the differentiation and apoptosis of B cells, which hence remain at the proliferative GC stage [9]. This is associated with diffuse large B cell lymphoma (DLBCL), which has been shown to play a central role in DLBCL pathogenesis [10]. Thus, targeting BCL6 repression represents a promising therapeutic strategy for treatment of B cell lymphomas [11].

At the molecular level, the protein comprises a DNA-binding C-terminal domain of six zinc fingers (ZF) followed by a central region of several hundred residues that are predicted to have little or no fixed 3D structure. The N-terminal domain is shared with other proteins of the so-called BTB-POZ [12] family (bric-a-brac tramtrack broad complex-Pox virus and zinc-finger). This from now on referred to as BTB domain is an evolutionary conserved protein–protein interaction motif found in 43 ZF transcription factors [13]. In all cases known to date normal activities of BTB-ZF proteins require BTB domain dimerization, and possibly also BTB-mediated oligomerization.

After dimerization, the BCL6 BTB domain forms two lateral grooves along the dimer interface which are required to recruit its corepressors. Corepressors that are known to interact with BCL6 are BCOR (BCL6 interacting corepressor) [14], SMRT (silencing mediator for retinoid and thyroid hormone receptor) [15–17] and NcoR (nuclear receptor corepressor) [16]. All these corepressors

* Corresponding author. Tel.: +34 953213057.
E-mail address: jmroldan@ujaen.es (J.M. Granadino-Roldán).

http://dx.doi.org/10.1016/j.jmgm.2014.04.003
1093-3263/© 2014 Elsevier Inc. All rights reserved.

	1	2	3	4	5	6	7	8	9	10	11	12	13	14	15	16	17
SMRT$^{1414-1430}$	L	V	A	T	V	K	E	A	**G**	**R**	**S**	**I**	**H**	**E**	**I**	**P**	**R**
NcoR$^{1351-1367}$	G	I	T	T	I	K	E	M	G	R	S	I	H	E	I	P	R
BCOR$^{498-514}$		R	S	E	I	I	S	T	A	P	S	S	W	V	V	P	G	P

Scheme 1. Structure-based sequence alignment of the SMRT, NcoR and BCOR BBDs showing the sequence numbering used throughout this work. Residues used to obtain a peptidomimetic in reference [21] are shown in bold, and those imitated by compound 79-6 in [20] in red.

bind in a mutually exclusive fashion using a 17 residue BCL6 binding domain (BBD) [18,19]. While the BBD domain is very similar between SMRT and NcoR, it completely differs for BCOR (see Scheme 1), although the X-ray structures [18,19] show a similar interaction mode between BCL6 and SMRT^{BBD} or BCOR^{BBD}.

Targeting the lateral groove with small molecules [20] or peptides [21] has already been demonstrated useful as a therapeutic strategy for DLBCL treatment. These successful approaches have been based on the X-ray structure of BCL6^{BTB} in complex with SMRT^{BBD} (PDB id. 1R2B) [18]. The X-ray structure of BCL6^{BTB} in complex with BCOR^{BBD} (PDB id. 3BIM) [19] has recently been reported and used together with that of the BCL6^{BTB}–SMRT^{BBD} complex by Guvench and MacKerell [22] to perform a computer-aided analysis of the interactions between BCL6 and these two corepressors applying the SILCS (site identification by ligand competitive saturation) method. To the best of our knowledge there are no available structures of the complex between BCL6^{BTB} and NcoR^{BBD}. Taking into account that all these three corepressors interact with the same zone of BCL6, this work has been aimed to identify a dynamic pharmacophore accounting for the interaction between BCL6^{BTB} and the corepressors SMRT^{BBD}, BCOR^{BBD} and NcoR^{BBD}. This pharmacophore can be used in a further step to screen commercially available databases in order to identify new compounds able to interrupt the interaction between BCL6^{BTB} and its corepressors.

Here, we report the obtainment of this pharmacophore using molecular dynamics (MD) simulations and free energy calculations of the complexes formed by BCL6 and the corepressors SMRT^{BBD}, BCOR^{BBD} and NcoR^{BBD}, taking into account the role of water molecules in the stability of these complexes.

2. Computational details

All the calculations described in this work were carried out at molecular mechanics level using the Amber ff12SB force field [23] with the AMBER v.12 suite of programs [24]. All simulations were performed under periodic boundary conditions in which long-range electrostatic interactions were treated using the particle-mesh-Ewald method [25] and the cut-off distance was kept to 10 Å to compute non bonded interactions. The solvent was considered explicitly using TIP3P water molecules in a cubic solvent box [26]. The analysis of the trajectories was done with the *cpptraj* [27] program within Ambertools 13 [24] and the MMPBSA.py script [28]. The binding free energies were calculated using the MMPBSA.py script, following the MMPB(GB)SA scheme [29]. Graphics were prepared with Origin 8.5 [30], figures and some of the analyses used the UCSF Chimera package [31], and LIGPLOT [32] was used to analyze and show interactions between BCL6^{BTB} and its corepressors.

2.1. Construction of BCL6-corepressor complexes

The initial structures of the complexes BCL6^{BTB}–SMRT^{BBD} and BCL6^{BTB}–BCOR^{BBD} were taken from the Protein Data Bank (http://www.rcsb.org/pdb) with the access codes 1R2B and 3BIM, respectively. The 1R2B structure comprises the BCL6^{BTB} homodimer complexed with two SMRT^{BBD} peptides and 130 oxygens of water molecules. On the other hand, the 3BIM structure shows four independent BCL6^{BTB} dimers within the crystal asymmetric unit, with each dimer associated with two BCOR^{BBD} oligopeptides. As the four dimers are very similar [19] we decided to work with just the first one described in the PDB file, which also includes 53 oxygens of water molecules. From now on we will label each chain in the BCL6^{BTB} dimer as chain A and B, with the BTB domain herein analyzed going from 5 to 129, while the corepressor chain interacting with the lateral groove of chain A will be labeled as chain C, and the corresponding one interacting with chain B will be labeled as chain D, both being numbered from 1 to 17 (see Scheme 1). In both cases BCL6^{BTB} chain B misses residue GLU^{129} and it was necessary to revert the engineered mutant residues C8Q, C67R and C84N, while in the case of 1R2B residue, ALA^{5}B was missing. The missing residues were added by superposing chains A and B with Chimera and manually editing the PDB file to copy the missing residues from chain A to chain B. Mutant residues were fixed by manually deleting their side chains and changing the remaining backbone atoms to pertain to the original sequence, and later on importing the whole structures with the *leap* module of AMBER v.12, which added the missing side chain atoms. Finally, the Reduce [33] software was used to place missing hydrogen atoms, side chain orientations and to assign tautomeric and protonation states of titratable residues.

On the other hand, the BCL6^{BTB}–NcoR^{BBD} complex was constructed by homology modeling using the 3D structure of BCL6^{BTB}-SMRT^{BBD} as template. The SMRT and NcoR proteins have an overall pairwise sequence identity of 45% and a BBD sequence identity of 70.6%, being the C-terminal part (from residue 9–17) identical. This high similarity between BBDs, together with the already mentioned fact that these 17 residues bind in a mutually exclusive fashion, allow us to propose a method to model NcoR which consists of obtaining the side chain coordinates of identical residues with the leap module of AMBER v.12, hence assuming that they exhibit the same fold as those of their template. Moreover, three of the five amino-acids in which SMRT^{BBD} and NcoR^{BBD} differ are solvent exposed (LEU^{1}, ALA^{3} and ALA^{8}) and the other two are the same amino acid (VAL^{2,5}) which is mutated to a similar slightly bigger amino acid (ILE^{2,5}).This will be complemented with a sufficiently long simulation timescale for these small changes to converge. Finally, TIP3P water molecules and counterions (where necessary) were added to the system, although it is important to emphasize that in all cases crystal waters were retained (for NcoR, those waters from the 1R2B PDB file).

2.2. Energy minimizations

The complexes with SMRT^{BBD} and BCOR^{BBD} were energy minimized to remove possible steric stress by the following multi-step procedure. First, waters and counterions, together with the added residues are minimized (GLU^{129}B in both cases and also ALA^{5}B for SMRT^{BBD}). Second, only backbone atoms are kept fixed lowering their restraints from 10 kcal mol^{-1} to 1 kcal mol^{-1} and later to 0.1 kcal mol^{-1}. Third, all atoms are allowed to move. For the complex with NcoR^{BBD} the protocol started with minimizing waters together with NcoR^{BBD} side chains, followed by the previously described steps 2 and 3. Each of the described steps consisted of 5000 cycles.

2.3. Molecular dynamics simulations

All MD simulations were performed at a constant temperature of 300 K by coupling the system to a thermal bath using a Langevin thermostat algorithm [34,35] with a collision frequency of 5 ps^{-1}. Time step was set to 1 fs during equilibration, and to 2 fs during production with bond lengths involving hydrogen atoms constrained to equilibrium lengths with the SHAKE algorithm [36].

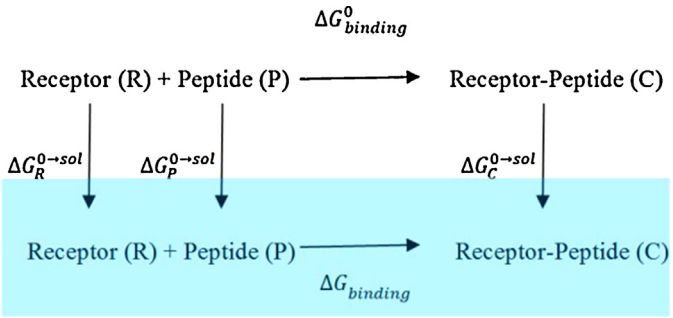

Fig. 1. Thermodynamic cycle used to obtain an expression for the total binding free energy.

MD equilibrations began by heating the minimized structures to 300 K over a period of 200 ps at a constant rate of 1.5 K ps^{-1} under the NVT ensemble. After the heating, equilibration involved 200 ps in the NPT ensemble (1 atm, 300 K) to increase the density of the system, using a weak-coupling algorithm analogous to temperature coupling [37]. Finally, production MD was performed during 100 ns at a constant temperature of 300 K in the NVT ensemble.

2.4. Energetic analyses

We used the MMPBSA.py program in order to obtain information from the decomposition of the energy among different groups of atoms during the trajectory. For this purpose, we used the last 5 ns of the MD with snapshots taken each 10 ps, to obtain the electrostatic (ELE) and van der Waals (VDW) interaction energies between each residue in the BBD of the corepressor and the whole $BCL6^{BTB}$. We also used the same snapshots to discern which residues of $BCL6^{BTB}$ interact most with those residues of the corepressor exhibiting best interaction energies.

2.5. Free energy calculations

Binding free energy calculations used the molecular mechanics generalized Born surface area (MMGBSA), and the molecular mechanics Poisson-Boltzmann surface area (MMPBSA) methodologies as implemented in the AMBER v.12 package [24]. Thus, these methods used the thermodynamic cycle depicted in Fig. 1 to obtain an expression for the total binding free energy that includes the solvation contributions:

$$\Delta G_{binding} = \Delta G^0_{binding} + \Delta G_C^{0\to solv} - \Delta G_R^{0\to solv} - \Delta G_P^{0\to solv}$$
$$= \Delta G^0_{binding} + \Delta G_C^{solv}$$

where the subscripts *C*, *R*, and *P* refer to complex, receptor and peptide, respectively. Also,

$$\Delta G^0_{binding} + \Delta G^0_C - \Delta G^0_R - \Delta G^0_P$$

where $\Delta G^0_{binding}$ is the binding free energy *in vacuo*:

$$\Delta G^0_{binding} = \Delta H^0_{binding} - T\Delta S^0_{binding}$$

The enthalpy contribution can by expressed as:

$$\Delta H^0_{binding} = \Delta H^0_{\text{int}} - \Delta H^0_{vdW} + \Delta H^0_{elec}$$

where ΔH^0_{int} is the internal, ΔH^0_{vdW} the noncovalent van der Waals and ΔH^0_{elec} the electrostatic molecular mechanics energies. On the other hand, ΔG^{solv} comprises the polar (ΔG_{polar}) and nonpolar ($\Delta G_{\text{nonpolar}}$) terms. The polar term can be calculated solving the Poisson–Boltzmann (PB) equation or by the generalized Born (GB) method. For the GB method we used the Onufriev approximation (igb = 5) [38]. Finally, the nonpolar part of the solvation term is calculated using the equation $\Delta G_{\text{nonpolar}} = \gamma\, SASA + \beta$, with SASA being the solvent-accessible surface area. In this work a one-trajectory protocol is used which means that the set of structures for the unbound receptor and ligand are extracted from the set of snapshots of the complex trajectory. This approximation avoids the calculation of separated trajectories for free receptor and ligand but it can be only applied when no significant conformational changes occur upon binding. This approximation can be considered valid in this case, as the starting X-ray structures for the MD runs are those of the established complexes. Within this approximation we have:

$$\Delta H^0_{\text{int}} = \Delta H^0_{C,\text{int}} - \Delta H^0_{R,\text{int}} - \Delta H^0_{P,\text{int}} = 0$$

The parameters used where: interior and exterior dielectric constants of 1 and 80, respectively; $\gamma = 0.005420$ kcal mol^{-1} and $\beta = 0.9200$ kcal mol^{-1} $Å^{-2}$ for PB calculations, while default values are used for GB calculations. The binding free energies for the complexes were calculated for the last 5 ns of MD using 1 snapshot for each 10 ps. The contribution of each residue to the total free energy of binding was analyzed using the MMGBSA decomposition protocol implemented in MMPBSA.py, using the same number of snapshots. Changes in internal entropy have been ignored, as our goal is not to reproduce absolute binding energies, but to quantify and analyze energy changes when essaying different corepressors.

2.6. Hydrogen bond analysis

The hydrogen bonds between each corepressor and $BCL6^{BTB}$ were characterized using *cpptraj* over the last 5 ns of simulation time. Parameters used to decide whether the hydrogen bond was established or not were: (1) hydrogen acceptor–donor distance of less than 3.5 Å and (2) acceptor–H–donor angles (θ_{HB}) of more than 120°. The percentage of structures in which the hydrogen bond satisfies both these conditions is quantified by a percentage of occupation. Values for the hydrogen bond angles are reported as 180 – θ_{HB}.

2.7. Water-mediated hydrogen bond analysis

In order to detect solvent molecules of interest from a pharmacophoric point of view, we performed a multi-step analysis which used the last 5 ns of MD (500 snapshots) and started with the generation with *cpptraj* of 4 occupancy grids for oxygen atoms in water, each grid centered around a part of the corepressor. The grid was computed for the whole simulation box and had a resolution of 0.5 $Å^3$. The grid was visualized with Chimera and those zones with a density of water ~4 times those of bulk water [39] were chosen for further analysis. This analysis was complemented with the use of the command *hbond* with *cpptraj* which now allows obtaining a list of those residues bridged by water and a time series of the waters bridging residues. The parameters used to decide if a hydrogen bond was established were the same as those described in the hydrogen bond analysis section.

3. Results and discussion

3.1. MD trajectory analysis

Fig. 2 shows some useful data to check the convergence of the MD trajectories. Thus, it can be seen how the root mean square deviation (RMSD) of backbone atoms and the MMPBSA and MMGBSA binding energies allow to consider all trajectories converged after around 25 ns (Fig. 2a and b). The atomic positional fluctuations (RMSF) of residues in each corepressor exhibit the expected

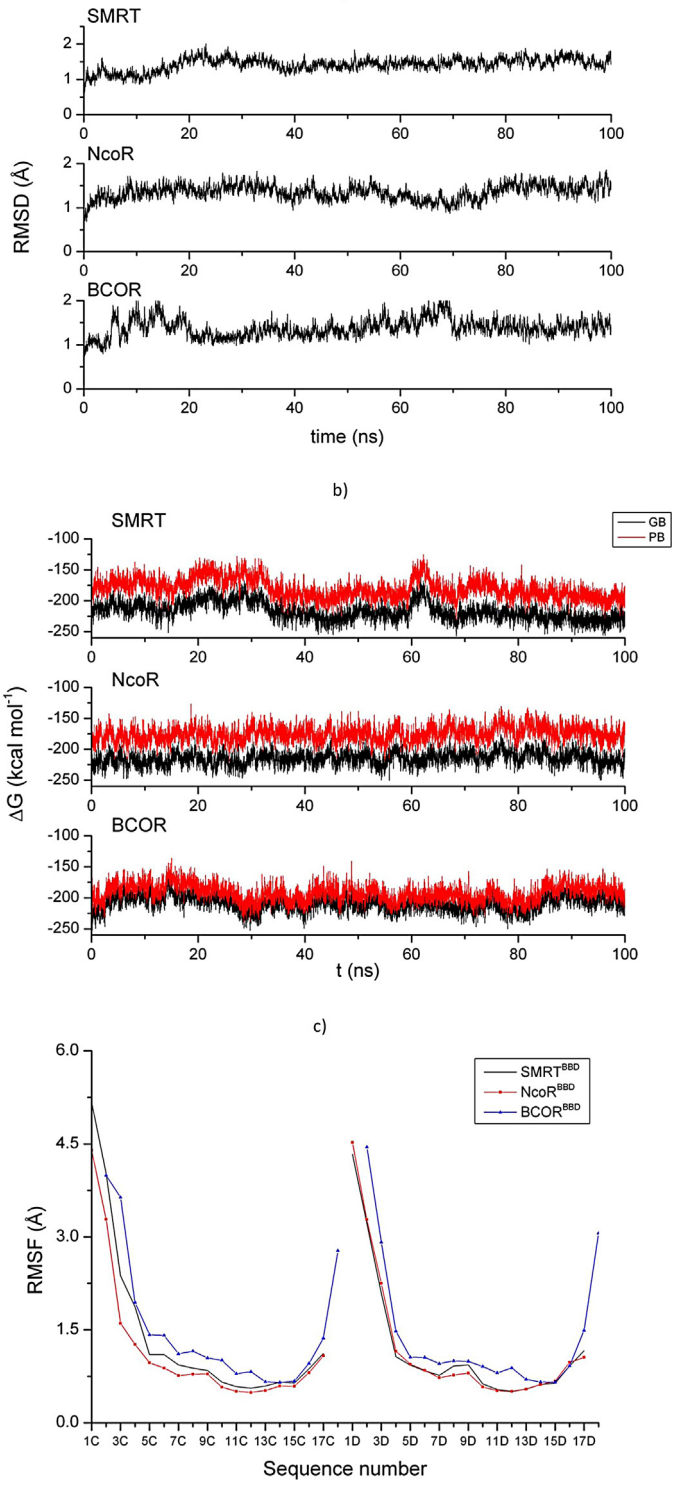

Fig. 2. (a) RMSD of the backbone atoms of $BCL6^{BTB}$ and each corepressor along the MD. (b) MMPBSA and MMGBSA $\Delta G_{binding}$ energies *versus* time. (c) Atomic positional fluctuations (RMSF) by residue for each chain of each corepressor.

trend, with those in the N- or C-terminal part having the highest values. In general both BBDs (chains C and D) show similar RMSF values, being these somewhat higher in the case of the $BCL6^{BTB}$–$BCOR^{BBD}$ complex (Fig. 2c) .In order to check that the predicted structure for the $BCL6^{BTB}$–$NcoR^{BBD}$ complex was reasonable, we obtained an averaged structure from the last 5 ns of each MD run for the $SMRT^{BBD}$ complex as well as the $NcoR^{BBD}$ complex, both shown superimposed in Fig. 3. As expected, taking into account

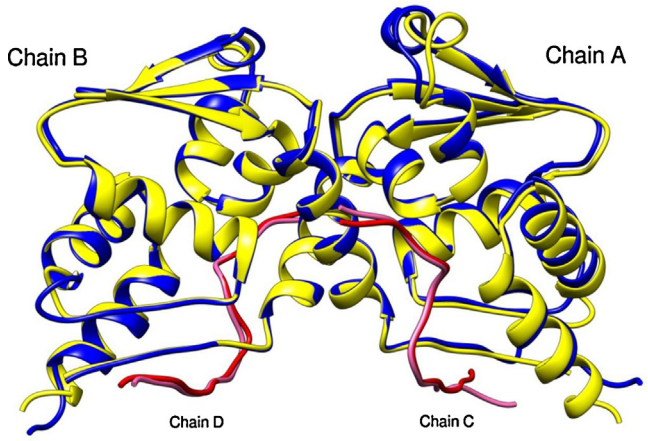

Fig. 3. Superposition of the structures averaged during the last 5 ns of MD of the $SMRT^{BBD}$ and $NcoR^{BBD}$ complexes. The $BCL6^{BTB}$ domain complexed with $SMRT^{BBD}$ is colored blue, while the corresponding with $NcoR^{BBD}$ is colored yellow. The $SMRT^{BBD}$ oligopeptide is colored red, and the $NcoR^{BBD}$ one is colored pink.

the sequence similarity between $SMRT^{BBD}$ and $NcoR^{BBD}$, the structures are very similar with the biggest differences appearing in the N-terminal part of each corepressor BBD.

3.2. Energetic analysis

The evolution of $\Delta G_{binding}$ with time, for the three complexes with the three previously described approaches to calculate the polar part of the solvation energy, is summarized in Fig. 2b. The trends are similar for all complexes, as it can also be seen in Table 1, which compares the $\Delta G_{binding}$ (ignoring the conformational entropy) with the experimental values determined by isothermal titration calorimetry (ITC) in ref. [18,19]. The absolute values for $\Delta G_{binding}$ are always lower in the case of PB and, although the subtle experimental differences between the three binding energies are not reproduced by any of the methods, it is worth pointing out that indeed PB and GB predict close values for the three studied systems. This is particularly interesting in the case of NcoR, as suggests that the proposed structure has been correctly modeled.

The contribution to the total $\Delta G_{binding}$ of each residue of the $BCL6^{BTB}$ and corepressor BBD is shown in Fig. 4. Focusing on $BCL6^{BTB}$, chains A and B show similar contributions and it can be seen how residues ILE^{9}, GLN^{10}, PHE^{11}, ASN^{21}, ARG^{24}, ARG^{28} and HIS^{116} stand out. These residues, together with ARG^{13} have previously been identified [18] to have side chains that make sizable contributions to the binding while not being conserved within the BTB ZF family of proteins. It has indeed been shown that the mutation N21 K impedes the binding with the SMRT corepressor, and the BTB ZF protein PLZF precisely has a lysine in that position; and it has also been shown that the mutation H116A decreases the affinity between $BCL6^{BTB}$ and $SMRT^{BBD}$ [18]. It can also be seen in Fig. 4 how the most remarkable residues of the corepressors as concerns $\Delta G_{binding}$ are HIS^{13}/HIS^{13}/TRP^{13} and ILE^{15}/ILE^{15}/VAL^{15}

Table 1
$\Delta G_{binding}$ (ignoring the conformational entropy), in kcal mol^{-1}, calculated following the MMPBSA and MMGBSA methodologies, along with experimental values. Entropic terms have been neglected.

Corepressor	PB	GB (igb = 5)	Experimental
SMRT	−197.67	−230.31	−6.78[a]
NcoR	−179.49	−220.70	−7.33[a]
BCOR	−188.18	−205.55	−8.06[b]

[a] Obtained from the k_d value given in reference [18].
[b] Obtained from the k_d value given in reference [19].

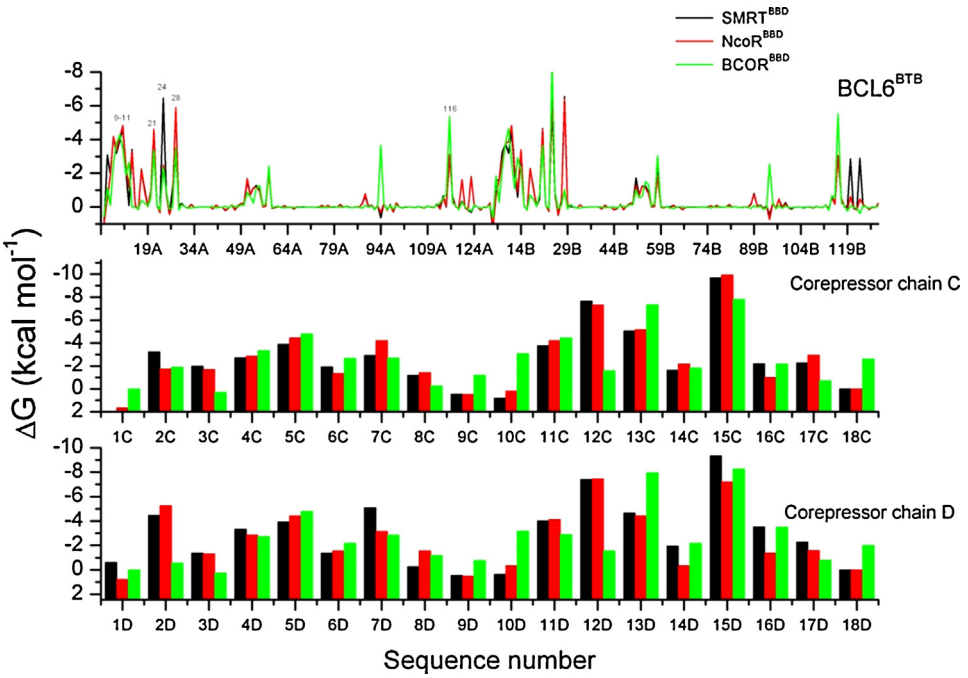

Fig. 4. Contribution of each residue of BCL6^{BTB} and corepressor^{BBD} domains to the total $\Delta G_{binding}$. (For interpretation of the references to color in this figure legend, the reader is referred to the web version of this article.)

Table 2
Vacuum interaction energies (kcal mol^{-1}) between each residue of the corepressor^{BTB} domain and the whole BCL6^{BBD}.

Sequence number	Corepressor								
	SMRT			NcoR			BCOR		
	VDW	ELE	TOTAL	VDW	ELE	TOTAL	VDW	ELE	TOTAL
1C	−0.69	2.83	2.15	−0.41	−25.01	−25.42			
2C	−3.23	−2.00	−5.23	−1.84	−0.69	−2.53	−0.58	−26.78	−27.36
3C	−1.80	−2.75	−4.55	−1.97	−1.77	−3.74	−0.38	2.04	1.66
4C	−3.50	−1.82	−5.32	−3.00	−3.43	−6.43	−3.10	−34.66	−37.76
5C	−2.71	−5.53	−8.23	−3.14	−5.22	−8.37	−3.07	−5.92	−8.99
6C	−2.69	11.84	9.14	−2.52	12.36	9.83	−2.57	−0.15	−2.72
7C	−4.18	−13.77	−17.95	−4.20	−43.30	−47.50	−3.64	−6.61	−10.25
8C	−1.77	−2.45	−4.22	−2.19	−1.62	−3.81	−1.70	−0.95	−2.65
9C	−1.51	−1.51	−3.02	−1.60	−1.07	−2.67	−2.54	−2.93	−5.47
10C	−6.18	1.88	−4.30	−6.60	3.12	−3.48	−3.47	−1.57	−5.04
11C	−4.47	−3.77	−8.24	−4.65	−4.71	−9.36	−4.05	−5.09	−9.13
12C	−7.89	−2.72	−10.61	−7.67	−2.07	−9.75	−3.33	−2.29	−5.62
13C	−6.45	−6.54	−12.99	−5.77	−6.66	−12.43	−8.12	−3.68	−11.80
14C	−1.54	−26.49	−28.02	−1.68	−31.52	−33.20	−2.38	−0.39	−2.77
15C	−6.23	−10.23	−16.46	−6.60	−9.97	−16.57	−5.01	−9.40	−14.41
16C	−2.21	−4.22	−6.43	−2.65	−0.27	−2.91	−2.20	−2.89	−5.09
17C	−2.24	−21.57	−23.81	−3.15	−24.07	−27.22	−1.77	−0.60	−2.36
18C							−1.48	−45.00	−46.48
1D	−0.53	−48.48	−49.01	−0.43	−25.25	−25.68	0.00	0.00	0.00
2D	−4.46	−7.52	−11.98	−4.97	−5.72	−10.69	−1.25	−20.46	−21.71
3D	−1.68	−1.45	−3.13	−1.78	−1.70	−3.48	−0.40	1.97	1.57
4D	−2.82	−2.53	−5.36	−2.79	−1.86	−4.65	−3.46	−28.32	−31.78
5D	−2.55	−4.33	−6.88	−2.93	−4.28	−7.21	−2.87	−5.85	−8.71
6D	−2.84	10.36	7.52	−2.97	10.26	7.30	−2.31	−0.34	−2.64
7D	−3.75	−52.14	−55.89	−4.29	−22.43	−26.72	−3.48	−6.24	−9.72
8D	−1.28	0.21	−1.06	−2.21	−2.26	−4.48	−2.19	−1.61	−3.80
9D	−1.73	−0.29	−2.02	−1.54	−1.26	−2.80	−2.29	−2.00	−4.29
10D	−6.45	6.96	0.51	−6.42	1.72	−4.70	−3.06	−1.29	−4.36
11D	−4.64	−4.58	−9.22	−4.43	−4.85	−9.29	−2.90	−4.71	−7.61
12D	−7.66	−1.95	−9.61	−7.68	−2.05	−9.73	−2.86	−2.68	−5.54
13D	−5.73	−6.29	−12.02	−5.81	−5.39	−11.20	−8.40	−4.79	−13.19
14D	−1.65	−35.44	−37.09	−2.08	−18.49	−20.57	−2.39	−0.57	−2.96
15D	−6.58	−8.88	−15.46	−6.92	−4.77	−11.69	−5.37	−9.86	−15.22
16D	−2.10	−4.91	−7.01	−2.50	−1.44	−3.94	−2.38	−4.54	−6.92
17D	−4.50	−14.10	−18.60	−3.42	−20.76	−24.18	−1.41	−1.57	−2.98
18D							−2.37	−12.02	−14.39

(SMRT/NcoR/BCOR from now on), while ILE^{12} stands out in the case of SMRT and NcoR. Cerchietti et al. have shown that the most important part within SMRT^{BBD} is that comprised by residues GLY^{9} to ARG^{17} [21], and obtained a small molecule inhibitor that imitates residues HIS^{13} and ILE^{15}. Besides, Ahmad et al. showed that the mutation S^{11}I^{12} → I^{11}S^{12} abrogates binding between BCL6^{BBD} and SMRT^{BTB} [18]. The analysis of Fig. 1S (which shows the side chain and backbone contributions of each residue to the total $\Delta G_{binding}$) confirms that residues 15 and 13 of all corepressors and residue ILE^{12} of SMRT and NcoR establish specific (*i.e.* side chain dependent) interactions with BCL6. Guvench and MacKerell also concluded about the importance of side chain interactions established by residue 15 for SMRT and BCOR and by residue 12 for SMRT [22]. It is also worth pointing out that the corepressors N-terminal part has THR^{4}/THR^{4}/GLU^{4}, VAL^{5}/ILE^{5}/ILE^{5} and GLU^{7}/GLU^{7}/SER^{7} as consensus residues with good $\Delta G_{binding}$ contributions.

The MMPB(GB)SA analysis can be complemented with an energetic vacuum per residue interaction analysis. Table 2 shows the interaction energies (VDW and ELE) between each of the residues of the corepressor and the whole BCL6^{BTB}. As expected, results follow the same trend as the $\Delta G_{binding}$ and a consensus proposal of outstanding residues could be corepressor residues 7, 13 and 15. These three residues present important van der Waals and electrostatic contributions. In order to know which residues of BCL6

Table 3
Hydrogen bonds formed between SMRT^{BBD}/NcoR^{BBD}/BCOR^{BBD} chain C and BCL6^{BTB} over the last 5 ns of the molecular dynamics. Shaded cells highlight side chains.

SMRT	NcoR	BCOR	BCL6	Avg. distance (Å)	Avg. angle (°)	% occupation
			ASP^{6}B OD1	2.89	29.0	47.4
		ARG^{2}C HH12[a]	ASP^{6}B OD2	2.96	32.1	29.0
			ASP^{6}B O	2.98	37.8	24.8
			ASP^{6}B OD1	2.93	32.1	43.0
		ARG^{2}C HH22[a]	ASP^{6}B OD2	2.93	30.5	25.0
			ASP^{6}B O	2.93	33.6	26.4
ALA^{3}C O			CYS^{8}B H	3.03	39.4	62.8
			ARG^{94}A HH21	2.85	27.7	32.2
		GLU^{4}C OE1[b]	ARG^{94}A HE	2.98	31.0	30.6
			ARG^{94}A HH21	2.89	30.4	34.0
			ARG^{94}A HH12	2.88	28.8	19.0
		GLU^{4}C OE2[b]	ARG^{94}A HH22	2.96	33.5	13.6
			ARG^{94}A HE	2.94	28.4	44.2
VAL^{5}C O			GLN^{10}B H	2.94	23.0	99.6
	ILE^{5}C O			2.88	21.1	100.0
		ILE^{5}C O		2.88	17.8	99.8
VAL^{5}C H			CYS^{8}B O	3.04	22.7	95.2
	ILE^{5}C H			2.99	27.4	98.0
		ILE^{5}C H		2.95	18.9	98.2
GLU^{7}C O			THR^{12}B H	3.03	30.2	94.4
	GLU^{7}C O			3.07	33.2	91.0
GLU^{7}C H			GLN^{10}B O	3.00	30.0	94.6
	GLU^{7}C H			2.96	24.5	95.8
		SER^{7}C H		2.94	21.8	99.4
SER^{11}C HG			HIS^{14}B ND1	2.90	17.3	100.0
	SER^{11}C HG			2.88	17.2	100.0
		SER^{11}C H	ASP^{17}B OD2	2.91	17.4	99.6
HIS^{13}C O			ASN^{21}B HD21	2.82	16.1	100.0
	HIS^{13}C O			2.80	16.6	100.0
		TRP^{13}C O		3.03	26.0	97.6
HIS^{13}C HE2			MET^{51}A O	3.08	29.6	89.2
	HIS^{13}C HE2			2.97	28.2	98.4
		TRP^{13}C HE1		3.08	31.7	66.6
GLU^{14}C OE1[c]			ARG^{24}B HH12	2.84	21.5	37.6
GLU^{14}C OE2[c]				2.83	21.3	58.2
	GLU^{14}C OE1			2.82	19.2	40.2
	GLU^{14}C OE2			2.82	19.6	56.2
ILE^{15}C O			ARG^{24}B HH11	2.86	17.2	100.0
	ILE^{15}C O			2.85	21.0	99.8
		VAL^{15}C O		2.89	18.6	99.6
ILE^{15}C H			ASN^{21}B OD1	3.04	15.9	98.2
	ILE^{15}C H			3.01	16.9	99.4
		VAL^{15}C H		2.94	17.6	99.8
ARG^{17}C O			ARG^{28}B HH22	2.95	27.0	74.6
ARG^{17}C OXT				2.98	34.4	66.6
ARG^{17}C OXT			ARG^{28}B HH12	2.93	31.7	59.8
	ARG^{17}C O		ARG^{28}B HH21	3.12	41.6	64.6
	ARG^{17}C OXT			2.87	20.3	89.8
		PRO^{18}C OXT	ARG^{24}B HE	2.89	25.1	76.6

[a] See Fig. 3S.
[b] See Fig. 5.
[c] See Fig. 4S.

interact most with the consensus selected residues in the corepressors, we performed a pairwise analysis, focusing on corepressor chain C, which can be visualized in Fig. 2S. As it can be seen, these residues interact with ARG^{13}, ASN^{21}, ARG^{24} and ARG^{28}, all of them previously identified as non-conserved and important residues of BCL6^{BTB}. In the case of HIS^{13}/HIS^{13}/TRP^{13} and ILE^{15}/ILE^{15}/VAL^{15} there appears an interaction with MET^{51}A, which is conserved to be ALA in other members of the BTB ZF family like PLZF, HIC-1, ZID, FAZF and MIZ-1.

3.3. Hydrogen bonds

MD trajectories allow us not only to check what hydrogen bonds are being established between a ligand and its receptor, but also to obtain information about its stability and also to detect dynamic bonds (*i.e.* the involved atoms are different at different times but they belong to the same residues). Even though each chain of the BCL6^{BTB} dimer is very similar to the other one, with RMSDs between superimposed backbone atoms of just 0.36 Å for the X-ray structure, and ~0.6 Å for those averaged during the last 5 ns of MD, there appear differences when comparing the hydrogen bonds established by chain A and B. Nevertheless, the most important and strong hydrogen bonds are shared by both chains, thus this observation just stresses the complexity of the interactions being established within the studied systems. For the sake of simplicity, we will center our discussion on chain C, while all the data related with chain D appears as supplementary information. Hence, Table 3 lists the hydrogen bonds established by SMRT^{BBD}/NcoR^{BBD}/BCOR^{BBD} chain C during the last 5 ns of the MD, together with their average distances, angles, and % of occupation, while Table 1S lists those established by chain D.

It is interesting to note that the BBD N-terminal part, which exhibits relatively low interaction energies, establishes important hydrogen bonds. BCOR^{BBD} ARG^{2} and GLU^{4} establish specific dynamic hydrogen bonds not described previously with ASP^{6}B and ARG^{94}B, respectively, which a total high % of occupation. These are a dynamic hydrogen bonds alternatively established with the OD1 and OD2 oxygens of ASP^{6}B and HH12, HE and HH12 hydrogens of ARG^{94}A (see Figs. 5 and 3S, for the hydrogen bonds of GLU^{4}C and ARG^{2}C, respectively). VAL^{5}/ILE^{5}/ILE^{5} and GLU^{7}/GLU^{7}/SER^{7} were previously proposed as important consensus residues from an energetic point of view, and it can be seen that they establish strong non-specific hydrogen bonds with GLN^{10}B, CYS^{8}B and THR^{12}B, with % of occupation of more than 90%.

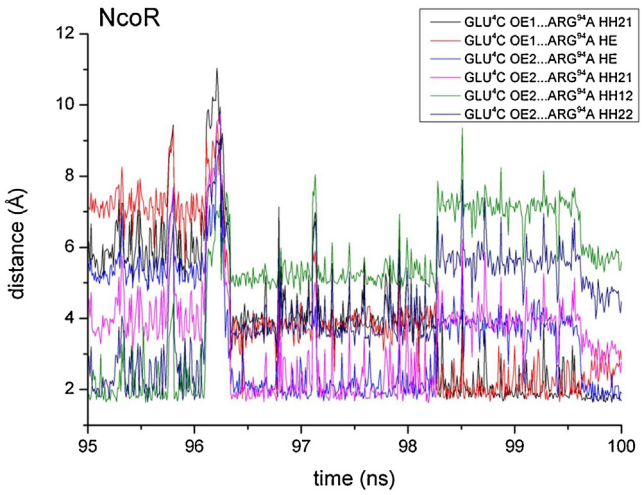

Fig. 5. Distances during the MD among the atoms involved in the hydrogen bond between GLU^{4}C of NcoR and ARG^{94}A of BCL6.

SER^{11}, together with PRO^{16}, are the only consensus sequence residues for all three corepressors, and it is known that the mutation S^{11}I^{12} → I^{11}S^{12} abrogates binding between BCL6^{BBD} and SMRT^{BTB}. Table 3 shows that indeed SER^{11} establishes specific hydrogen bonds with HIS^{14}B (SMRT^{BBD} and NcoR^{BBD}) or ASP^{17}B (BCOR^{BBD}) with % of occupation of 100%/100%/99.6% (SMRT^{BBD}/NcoR^{BBD}/BCOR^{BBD}).

Corepressor residues 13 and 15, apart from establishing strong van der Waals contacts (see Table 2), also exhibit important hydrogen bonds with the BCL6^{BTB} non-conserved residues ASN^{21}, ARG^{24} and MET^{51}. These hydrogen bonds, besides, are in all cases specific (by the BCL6 side or by the corepressor side) and with very high % of occupation (which is lower, 66.6%, in one case for BCOR). GLU^{14} establishes in the case of SMRT and NcoR a specific dynamic hydrogen bond with ARG^{24}, whose interacting atom distances are shown in Fig. 4S.

Table 4
Water-mediated hydrogen bonds formed between SMRT^{BBD}/NcoR^{BBD}/BCOR^{BBD} chain C and BCL6^{BTB} over the last 5 ns of the molecular dynamics. Shaded cells highlight side chains. Numbers correspond to the most stable hydrogen bond established by the oxygen in water.

SMRT	NcoR	BCOR	WATER	BCL6	Avg. distance (Å)	Avg. angle (°)	% occupation
GLU^{7}C OE1, OE2					3.03	34.7	99.2
			296				
	GLU^{7}C OE1, OE2				3.04	34.5	99.4
		SER^{7}C O	5343	ARG^{13}B HH22, HH12, HH11	3.02	32.5	64.2
GLY^{9}C O					3.03	34.7	99.2
			296				
	GLY^{9}C O				3.04	34.5	99.4
		ALA^{9}C O	5343		3.02	32.5	64.2
			291[a]	ASN^{21}B OD1; ASP^{17}B OD2	2.98	30.7	98.8
ARG^{10}C HH12, HH21, HH22, HE							
	ARG^{10}C HH12, HH21, HH22, HE				2.99	31.6	99.4
GLU^{14}C OE1, OE2			151 different waters	ARG^{24}B HH21, HH22, HE	3.00	31.8	89.2
	GLU^{14}C OE1, OE2		150 different waters		3.05	32.1	81.6
			61 different waters[b]	SER^{27}B HG	2.80	20.3	86.4
ARG^{17}C O, OXT							

[a] See Fig. 6.
[b] See Fig. 7.

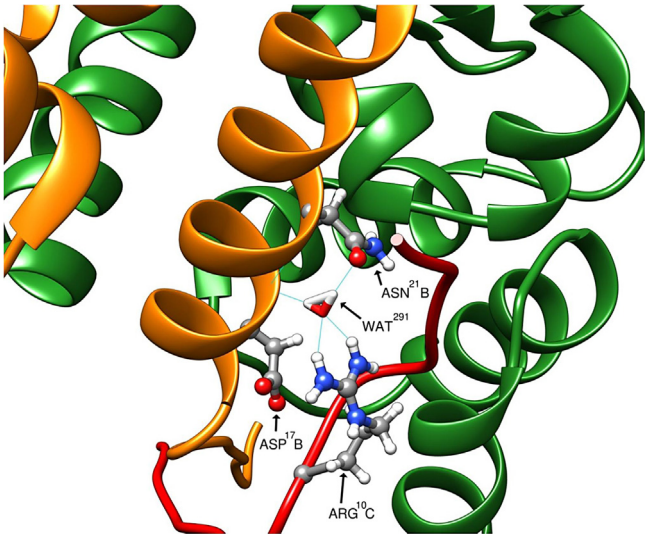

Fig. 6. Last snapshot of the MD trajectory of the BCL6^{BTB}–SMRT^{BBD} complex, focusing on WAT^{291}.

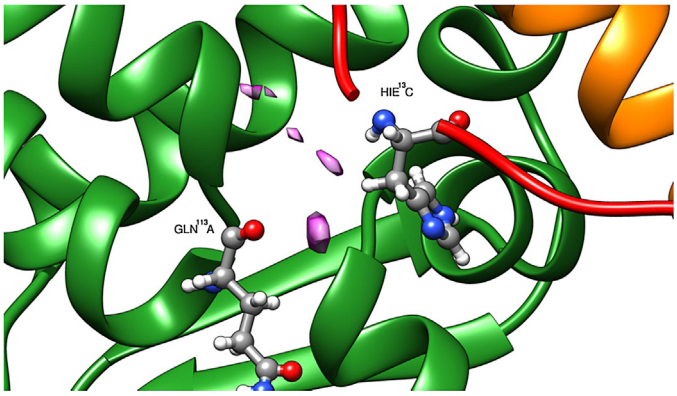

Fig. 7. Visualization with Chimera of the zones from the occupancy grid obtained with *cpptraj* with a density of water ~4 times those of bulk water (in pink) around ARG^{17}C. (For interpretation of the references to color in this figure legend, the reader is referred to the web version of this article.)

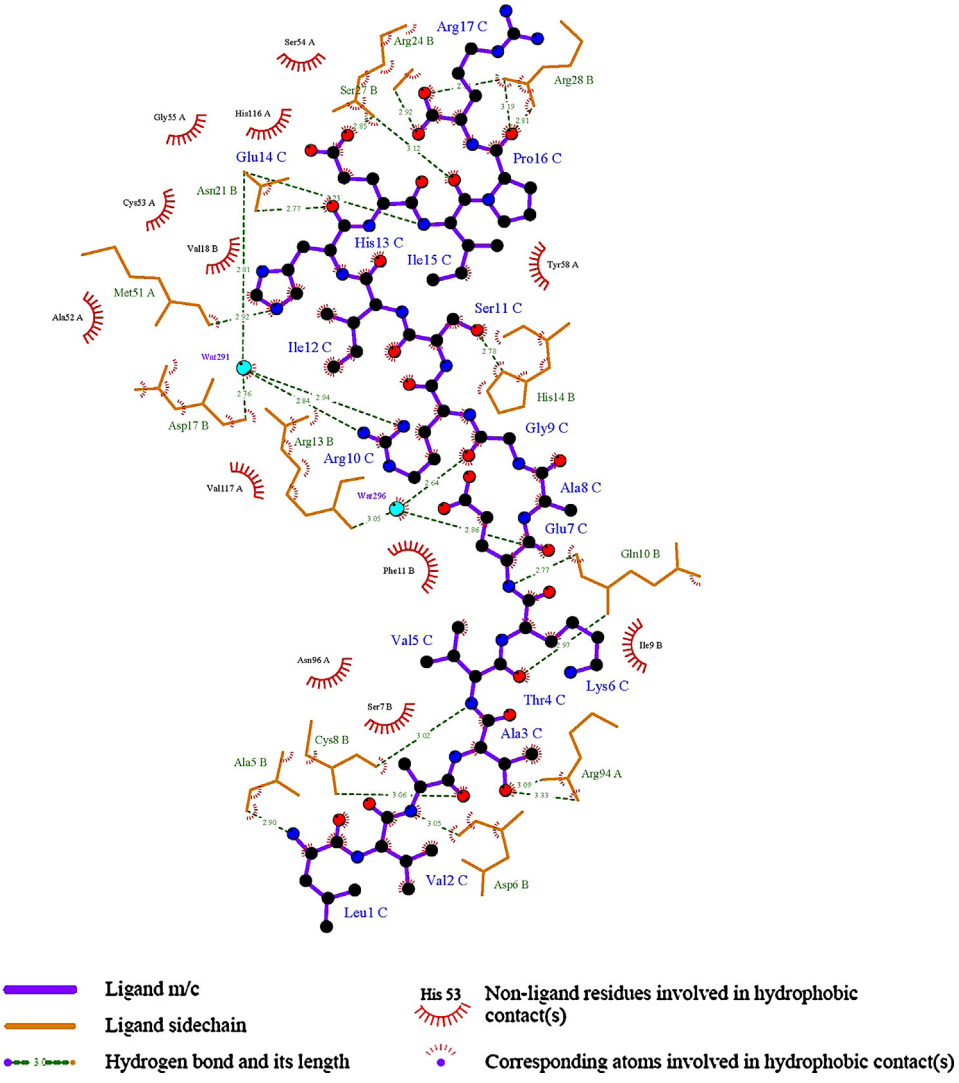

Fig. 8. Schematic drawing of the contacts found from the last snapshot of the MD between the BCL6 BTB domain and SMRT^{BBD} chain C.

Table 5
Summary of important residues shared by $SMRT^{BBD}$, $NcoR^{BBD}$ and $BCOR^{BBD}$ along with the major type of interaction they establish with BCL6.

Sequence number		4	5	7	11	13	15
Type of interaction	van der Waals	√	√	√		√	√
	Hydrogen bond		√	√	√	√	√

3.4. Water-mediated hydrogen bonds

Tables 4 and 2S compile information about the water mediated hydrogen bonds found throughout the MD trajectory for chains C and D, respectively. We must emphasize that the MMPB(GB)SA analysis did not include explicit water molecules. Water molecules have been numbered as they appear in the MD coordinate file. As before, for the sake of simplicity we will focus our analysis to those water-mediated hydrogen bonds established by chain C. As can be seen in Table 4 these hydrogen bonds are highly dynamic and specific. Ghetu et al. have already described a conserved water-mediated interaction of $ARG^{13}B$ with $GLU^{7}C$ and $GLY^{9}C/ARG^{13}B$ with $SER^{7}C$ and $ALA^{9}C$ (SMRT/BCOR) [19]. This group of water-mediated hydrogen bonds is also seen in the MD trajectory for the $BCL6^{BTB}$–$Ncor^{BBD}$ complex, with % of occupation of 99.4%. This % of occupation is lower for the corresponding $BCOR^{BBD}$ complex (64.2%), although the water-mediated hydrogen bond is being established during the whole 100 ns trajectory (the crystallographic water, WAT^{313}, moves apart but other water molecules establish the hydrogen bond, being the last one WAT^{5343}).

The remaining water-mediated hydrogen bonds are not seen in the case of the $BCL6^{BTB}$–$BCOR^{BBD}$ complex. These are established between $ARG^{10}C$, $ASP^{17}B$ and $ASN^{21}B$ (one crystallographic water, WAT^{291}), and between $GLU^{14}C$ with $ARG^{24}B$ (151 and 150 different waters for SMRT and NcoR, respectively). Fig. 6 shows the last snapshot of the MD for the complex $BCL6^{BTB}$–$SMRT^{BBD}$ focusing of WAT^{291}. The analysis of the occupancy grid shown in Fig. 7 (density of water ~4 times those of bulk water) confirmed that zone shown in pink to be occupied by 61 different waters bridging $ARG^{17}C$ and $SER^{27}B$, with a % of occupation of 86.4. This high density zone was only seen in the case of the $BCL6^{BTB}$–$SMRT^{BBD}$ complex.

3.5. Pharmacophoric hypothesis

Table 5 lists a summary of important residues shared by $SMRT^{BBD}$, $NcoR^{BBD}$ and $BCOR^{BBD}$, emphasizing with bold typography those interactions established mostly by side chains. As it is usual in protein–protein interactions the contact surface between the lateral groove of $BCL6^{BTB}$ and each BBD is large and has different hot spots, thus it is usual the existence of residues that are important from a structural point of view because they do not make the most important interactions. We have used a global analysis which includes MMPB(GB)SA, energetic pairwise analysis, hydrogen bonds and water-mediated hydrogen bonds, together with a visualization of the interactions identified by LIGPLOT (shown in Fig. 8 and Figs. 5S–9S) to propose a consensus global pharmacophore consisting of 14 pharmacophoric points. There are 5 hydrophobic points, 3 hydrogen acceptors, 5 hydrogen donors and 1 pharmacophoric point to mimic $WAT^{296}/WAT^{296}/WAT^{5343}$, which can be considered hydrogen donor or acceptor (the coordinates of the pharmacophoric points can be obtained upon request). These pharmacophoric points are shown in Fig. 9, where it is clear that the large contact surface can be mimicked by two groups of pharmacophoric points which coincide with corepressor residues 4–11 and 11–15. Hence, we can consider the pharmacophoric point for residue SER^{11} (shared by all three corepressors) a hinge pharmacophoric point. Thus, our analysis points to the possibility of searching for 2 small molecule inhibitors, instead of one, in order to inhibit BCL6: one molecule mimicking 8 pharmacophoric points, and the other one 7, using the hydrogen donor pharmacophoric point from SER^{11} in any or both of the searches. This conclusion points to a codrug administration as a possible novel strategy for inhibiting BCL6. Work is in progress in this direction.

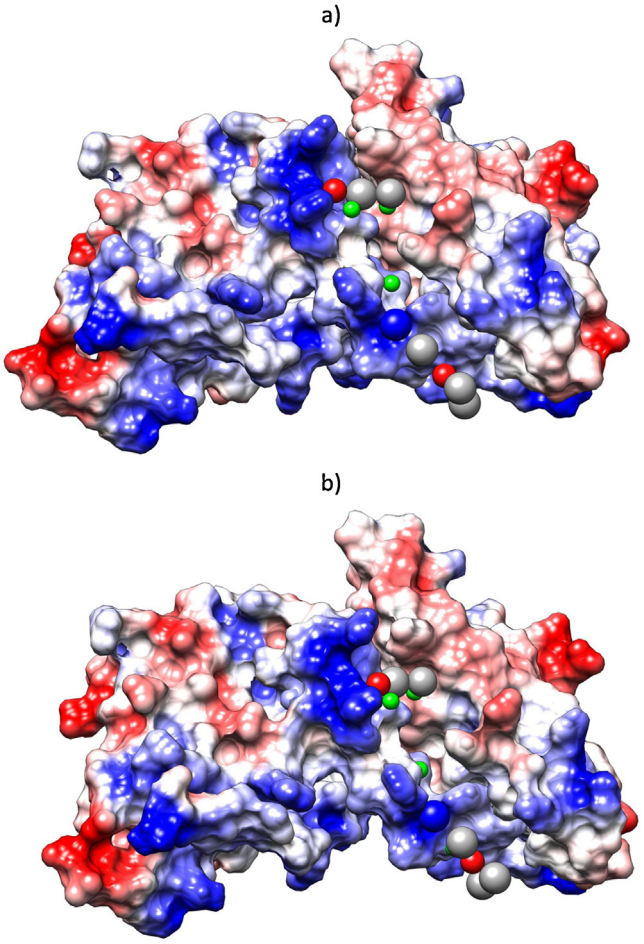

Fig. 9. Spatial representation of the proposed pharmacophoric points. (a) Centered around corepressor residues 4–11; (b) Centered around corepressor residues 11–15. In color gray the hydrophobic points, in red the hydrogen acceptors, in green the hydrogen donors, and in blue the water molecule.

4. Conclusions

Molecular dynamics simulations of the complexes between $BCL6^{BTB}$ and $SMRT^{BBD}$, $NcoR^{BBD}$ or $BCOR^{BBD}$ were performed with the aim of achieving a better understanding of the interactions between the protein and its corepressors. The comparison between results for the $BCl6^{BTB}$–$SMRT^{BBD}$ complex and the $BCL6^{BTB}$–$NcoR^{BBD}$ one supports the validity of the proposed modeled structure for the latter is correct. Results from MMPBSA and MMGBSA, which predict close values for the three studied systems, point to the same conclusion. As expected, most interactions already observed were conserved through the MD simulation, while the MD simulation provides additional information about the hydrogen bonds (% of occupation) and allows performing an energetic analysis. Thus, our results agree with the experiments in that, on the one hand, the sequence GLY^{9}–ARG^{17} is important for $SMRT^{BBD}$ binding [18,21], and on the other hand deletion of residues LEU^{1}–GLU^{7} abrogates $BCL6^{BTB}$–$SMRT^{BBD}$ complex formation. We propose, in agreement with Cerchietti et al. [20], that corepressor residues 13–15 are important, while our results, which

include also information regarding complexes of $BCL6^{BTB}$ with $NcoR^{BBD}$ and $BCOR^{BBD}$, allow us to expand that proposal. Focusing on the search for a consensus pharmacophore we propose, from an energetic point of view, residues 4, 5, 7, 13 and 15. We also propose as important residue SER^{11}, which establishes a specific dynamic hydrogen bond with HIS^{14} (SMRT, NcoR) or ASP^{17} (BCOR). Our analysis has included also water molecules, and we have found (in agreement with experimental results), one water molecule with importance for complex formation. Our proposal, therefore, would be to work with two pharmacophores, each one centered in one part of the $BCL6^{BTB}$ lateral groove surface, one consisting of 8 pharmacophoric points, and the other one of 7.

In summary, the present work is intended to be considered as a further step in the modeling of drugs mimicking $BCL6^{BTB}$–corepressor complexes, performing a global theoretical approach which analyses the dynamics of the three known BCL6 corepressors complexed with the DLBCL related protein BCL6.

Acknowledgements

The authors would like to thank the referees for helping to improve this work. It has been supported by the Ministerio Español de Ciencia y Tecnología (project CTQ2011-29285-C02-02) and the Generalitat de Catalunya (project 2009SGR1308). J.M.G. thanks the Universidad de Jaén (*Ayuda a personal investigador de la UJA para estancias en otros centros de investigación*) and A.M.R. & A.G.M. for fruitful discussions.

Appendix A. Supplementary data

Supplementary data associated with this article can be found, in the online version, at http://dx.doi.org/10.1016/j.jmgm.2014.04.003.

References

[1] C.C. Chang, B.H. Ye, R.S. Chaganti, R. Dalla-Favera, BCL-6, a POZ/zinc-finger protein, is a sequence-specific transcriptional repressor, PNAS. 93 (1996) 6947–6952.
[2] A.L. Dent, A.L. Shaffer, X. Yu, D. Allman, L.M. Staudt, Control of inflammation, cytokine expression, and germinal center formation by BCL-6, Science 276 (1997) 589–592.
[3] B.H. Ye, G. Cattoretti, Q. Shen, J. Zhang, N. Hawe, R. de Waard, et al., The BCL-6 proto-oncogene controls germinal-centre formation and Th2-type inflammation, Nat. Gen. 16 (1997) 161–170.
[4] B.W. Baron, M. Desai, L.J. Baber, L. Paras, Q. Zhang, A. Sadhu, et al., BCL6 can repress transcription from the human immunodeficiency virus type I promoter/enhancer region, Genes Chromosomes Cancer 19 (1997) 14–21.
[5] S. Parekh, G. Prive, A. Melnick, Therapeutic targeting of the BCL6 oncogene for diffuse large B-cell lymphomas, Leuk. Lymphoma 49 (2008) 874–882.
[6] R.T. Phan, R. Dalla-Favera, The BCL6 proto-oncogene suppresses p53 expression in germinal-centre B cells, Nature 432 (2004) 635–639.
[7] S.M. Ranuncolo, J.M. Polo, J. Dierov, M. Singer, T. Kuo, J. Greally, et al., Bcl-6 mediates the germinal center B cell phenotype and lymphomagenesis through transcriptional repression of the DNA-damage sensor ATR, Nat. Immunol. 8 (2007) 705–714.
[8] G. Cattoretti, R. Shaknovich, P.M. Smith, H.M. Jack, V.V. Murty, B. Alobeid, Stages of germinal center transit are defined by B cell transcription factor coexpression and relative abundance, J. Immunol. 177 (2006) 6930–6939.
[9] F. Jardin, P. Ruminy, C. Bastard, H. Tilly, The BCL6 proto-oncogene: a leading role during germinal center development and lymphomagenesis, Pathol. Biol. (Paris) 55 (2007) 73–83.
[10] G. Cattoretti, L. Pasqualucci, G. Ballon, W. Tam, S.V. Nandula, Q. Shen, et al., Deregulated BCL6 expression recapitulates the pathogenesis of human diffuse large B cell lymphomas in mice, Cancer Cell. 7 (2005) 445–455.
[11] J.M. Polo, T. Dell'Oso, S.M. Ranuncolo, L. Cerchietti, D. Beck, G.F. Da Silva, et al., Specific peptide interference reveals BCL6 transcriptional and oncogenic mechanisms in B-cell lymphoma cells, Nat. Med. 10 (2004) 1329–1335.
[12] V.J. Bardwell, R. Treisman, The POZ domain: a conserved protein–protein interaction motif, Genes Dev. 8 (1994) 1664–1677.
[13] P.J. Stogios, G.S. Downs, J.J. Jauhal, S.K. Nandra, G.G. Prive, Sequence and structural analysis of BTB domain proteins, Genome Biol. 6 (2005) R82.
[14] K.D. Huynh, W. Fischle, E. Verdin, V.J. Bardwell, BCoR, a novel corepressor involved in BCL-6 repression, Genes Dev. 14 (2000) 1810–1823.
[15] P. Dhordain, O. Albagli, R.J. Lin, S. Ansieau, S. Quief, A. Leutz, et al., Corepressor SMRT binds the BTB/POZ repressing domain of the LAZ3/BCL6 oncoprotein, PNAS 94 (1997) 10762–10767.
[16] K.D. Huynh, V.J. Bardwell, The BCL-6 POZ domain and other POZ domains interact with the co-repressors N-CoR and SMRT, Oncogene 17 (1998) 2473–2484.
[17] C.W. Wong, M.L. Privalsky, Components of the SMRT corepressor complex exhibit distinctive interactions with the POZ domain oncoproteins PLZF PLZF-RARalpha, and BCL-6, J. Biol. Chem. 273 (1998) 27695–27702.
[18] K.F. Ahmad, A. Melnick, S. Lax, D. Bouchard, J. Liu, C.L. Kiang, et al., Mechanism of SMRT corepressor recruitment by the BCL6 BTB domain, Mol. Cell. 12 (2003) 1551–1564.
[19] A.F. Ghetu, C.M. Corcoran, L. Cerchietti, V.J. Bardwell, A. Melnick, G.G. Prive, Structure of a BCOR corepressor peptide in complex with the BCL6 BTB domain dimer, Mol. Cell 29 (2008) 384–391.
[20] L.C. Cerchietti, A.F. Ghetu, X. Zhu, G.F. Da Silva, S. Zhong, M. Matthews, et al., A small-molecule inhibitor of BCL6 kills DLBCL cells in vitro and in vivo, Cancer Cell 17 (2010) 400–411.
[21] L.C. Cerchietti, S.N. Yang, R. Shaknovich, K. Hatzi, J.M. Polo, A. Chadburn, et al., A peptomimetic inhibitor of BCL6 with potent antilymphoma effects in vitro and in vivo, Blood 113 (2009) 3397–3405.
[22] O. Guvench, A.D. MacKerell Jr., Computational fragment-based binding site identification by ligand competitive saturation, PLoS Comput Biol. 5 (2009) e1000435.
[23] V. Hornak, R. Abel, A. Okur, B. Strockbine, A. Roitberg, C. Simmerling, Comparison of multiple Amber force fields and development of improved protein backbone parameters, Protein Struct. Funct. Bioinf. 65 (2006) 712–725.
[24] D. Case, T.A. Darden, T.E. Cheatham, C. Simmerling, J. Wang, R. Duke, et al., Amber 12, University of California, San Francisco, 2012.
[25] T. Darden, D. York, L. Pedersen, Particle mesh Ewald: An N log(N) method for Ewald sums in large systems, J. Chem. Phys. 98 (1993) 10089–10092.
[26] W.L. Jorgensen, J. Chandrasekhar, J.D. Madura, R.W. Impey, M.L. Klein, Comparison of simple potential functions for simulating liquid water, J. Chem. Phys. 79 (1983) 926–935.
[27] D.R. Roe, T.E. Cheatham, PTRAJ and CPPTRAJ: software for processing and analysis of molecular dynamics trajectory data, J. Chem. Theory Comput. (2013).
[28] B.R. Miller, T.D. McGee, J.M. Swails, N. Homeyer, H. Gohlke, A.E. Roitberg, MMPBSA.py: an efficient program for end-state free energy calculations, J. Chem. Theory Comput. 8 (2012) 3314–3321.
[29] P.A. Kollman, I. Massova, C. Reyes, B. Kuhn, S. Huo, L. Chong, et al., Calculating structures and free energies of complex molecules: combining molecular mechanics and continuum models, Acc. Chem. Res. 33 (2000) 889–897.
[30] Origin (OriginLab, Northampton, MA) OriginLab, Northampton, MA.
[31] E.F. Pettersen, T.D. Goddard, C.C. Huang, G.S. Couch, D.M. Greenblatt, E.C. Meng, et al., UCSF Chimera – a visualization system for exploratory research and analysis, J. Comput. Chem. 25 (2004) 1605–1612.
[32] A.C. Wallace, R.A. Laskowski, J.M. Thornton, LIGPLOT: a program to generate schematic diagrams of protein–ligand interactions, Prot. Eng. 8 (1995) 127–134.
[33] J.M. Word, S.C. Lovell, J.S. Richardson, D.C. Richardson, Asparagine and glutamine: using hydrogen atom contacts in the choice of side-chain amide orientation, J. Mol. Biol. 285 (1999) 1735–1747.
[34] B.P. Uberuaga, M. Anghel, A.F. Voter, Synchronization of trajectories in canonical molecular-dynamics simulations: observation, explanation, and exploitation, J. Chem. Phys. 120 (2004) 6363–6374.
[35] D.J. Sindhikara, S. Kim, A.F. Voter, A.E. Roitberg, Bad seeds sprout perilous dynamics: stochastic thermostat induced trajectory synchronization in biomolecules, J Chem Theory Comput. 5 (2009) 1624–1631.
[36] J.-P. Ryckaert, G. Ciccotti, H. Berendsen, Numerical integration of the cartesian equations of motion of a system with constraints: molecular dynamics of n-alkanes, J. Comput. Phys. 23 (1977) 327–341.
[37] H.J.C. Berendsen, J.P.M. Postma, W.F. Gunsteren, V.A. DiNola, J.R. Haak, Molecular dynamics with coupling to an external bath, J. Chem. Phys. 81 (1984) 3684–3690.
[38] A. Onufriev, D. Bashford, D.A. Case, Exploring protein native states and large-scale conformational changes with a modified generalized born model, Protein Struct. Funct. Bioinf. 55 (2004) 383–394.
[39] T.E. Cheatham, P.A. Kollman, Molecular dynamics simulations highlight the structural differences among DNA:DNA, RNA:RNA, and DNA:RNA hybrid duplexes, JACS 119 (1997) 4805–4825.